

Simulation results on a real-time in water tritium monitor [★]

C.D.R. Azevedo^{a,*}, A. Baeza^b, E. Chauveau^c, J.A. Corbacho^b, V. Delgado^b, J. Díaz^d, J. Domange^c, C. Marquet^c, M. Martínez-Roig^d, F. Piquemal^c, A. Rodríguez^b, J.F.C.A. Veloso^a and N. Yahlali^d

^a*I3N, Physics Department, University of Aveiro, Campus Universitário de Santiago, 3810-193 Aveiro, Portugal*

^b*Universidad de Extremadura, Laboratorio de Radioactividad Ambiental. Servicio de apoyo a la investigación, Cáceres, Spain*

^c*Université de Bordeaux and CNRS, CENBG, Gradignan Cedex, France*

^d*Instituto de Física Corpuscular, Centro mixto CSIC-Universidad de Valencia, Paterna, Spain*

ARTICLE INFO

Keywords:

tritium in water
real-time monitor
nuclear power plant
environmental safety

ABSTRACT

The low energy beta emission resulting from the tritium decay is a concern from the health and governmental entities in order to keep the As Low As Reasonably Achievable (ALARA) principle. Several legislation and regulation directives have been published defining the maximum concentration in water for human consumption, for example, 100 Bq/L by European directive 2013/51/Euratom and 740 Bq/L by the U.S. Environmental Protection Agency.

The challenge of the tritium decay detection is due to its weak emission requiring high sensitive devices or the most used technique, laboratory analysis using Liquid Scintillation Counting, which can take up to 4 days to achieve the low level sensitivity required by the legislation. In this work we present the simulation studies and ideas for an in-water Tritium real-time monitor based on optical scintillation fibbers. Conservative calculations allows to preview a 100 Bq/L sensitivity with 40 Bq/L of activity resolution by using a modular detector composed by 5 detection "cells" containing around 350 fibers each but passive/active shielding against natural/cosmic background as also a water purifying system is mandatory to reach such sensitivity.

1. Introduction

Tritium, a hydrogen isotope, is produced by neutron capture in nuclear power plants mainly in the water coolant and moderator, in quantities depending on the reactor type, i.e., Light-water-moderated reactors (LWR), Pressurized water reactors (PWR), Pressurized Heavy Water Reactor (PHWR), etc. The tritium produced in the coolant is partially or totally released in the air or in the water and in the latter case the dominant form is through tritiated water (HTO or T₂O) [1]. Despite the low energy beta emission from tritium decay (average emission energy is 5.7 keV and maximum 18 keV, see Figure 2) which cannot penetrate the skin, several state regulations have been released in order to regulate the maximum quantity of tritium in drinking water as for example, the U.S. Environmental Protection Agency (EPA) that sets a maximum of 740 Bq/L [2] or the E.U. Council Directive 2013/51/Euratom which establishes the limit to 100 Bq/L [3]. For such low required limits the mostly used technique is the Liquid Scintillation Counting (LSC) which produces toxic waste and requires sample collection, preparation and analysis which takes about 2 days. Real-time monitors based on solid scintillators have been proposed in several works, e.g. [4–6] obtaining detection limits in the order of dozens of kBq/L which is 2 orders of magnitude higher than the limit required by the E.U. directive. In 1998 J.W. Berthold and L.A. Jeffers [7] proposed the use of scintillating fibers with

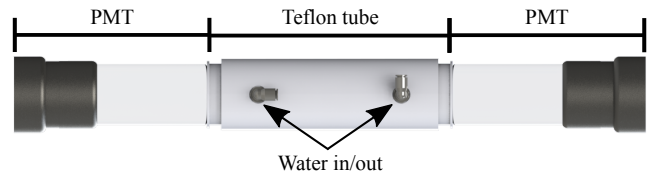


Figure 1: The TRITIUM-1 prototype setup studied and developed in this work

2% of fluor doped fiber clad. Unfortunately the authors concluded that their system was unable to comply with the U.S. EPA required sensitivity, finding in addition several issues related to the stability of fluor-doped clad immersed in water.

In this work the simulation studies of a real-time tritium monitor based on unclad scintillation fibers is presented. This monitor is being developed by the INTERREG SUDOE TRITIUM Project [8, 9] aiming to achieve the 100 Bq/L sensitivity required by the E.U. directive.

2. The setup

In order to measure the tritium activity in water, the setup presented in Figure 1 was conceived. The central part, from now on denominated as "cell", is a teflon (PTFE) tube containing scintillating fibers (Saint-Gobain Crystals BCF-10) immersed in water. The teflon material was chosen in order to maximize the optical photon reflection on the inner surface of the tube. Also, its mechanical properties allows to seal it against acrylic (PMMA) disks (the windows for light transmission to photosensors) by just applying pressure on

[★]This document is the results of the research project funded by INTERREG-SUDOE program through the project TRITIUM - SOE1/P4/E0214.

*Corresponding author

✉ cdazevedo@ua.pt (C.D.R. Azevedo)

ORCID(s): 0000-0002-0012-9918 (C.D.R. Azevedo)

the external walls of the tube using Hercules clamps. The cell also contains water inlet and outlet in order to keep a constant water flux. Inside the cell, 2 mm diameter round fibers, specially ordered unclad, are placed. According to the manufacturer, the clad has a thickness of 3% of the nominal fiber diameter [10]. The use of a fiber clad would prevent its use for this application as the beta emission from tritium are not energetic enough to reach the fiber core and in the eventual cases that this occurs, the energy of the particle would be strongly decreased in the clad. Indeed, as the refraction index of water is lower than that of PMMA, having the fiber core surrounded by water increases the fiber numeric aperture ($\theta_C \approx 56^\circ$) and thus increase the number of photons guided in the fiber due to total internal reflection. Although in this setup we are not interested in reading-out just single fibers but rather to maximize the number of detected photons, we must include the photons travelling in water that are not guided in the fibers.

The 2 mm diameter fibers were also been chosen in order to maximize the detection area in contact with water. Obviously lower diameters could be used allowing for a higher packing density but the water flux between fibers could be limited and thus requiring the use of fiber spacers that should increase the complexity of the detector construction.

In order to read out the fiber scintillation light, Hamamatsu R2154-02 PMTs were used. At present an analogous system using SiPMs is being studied.. PMTs offer advantage over SiPMs in price (for the same sensitive area), lower dark-counts, low number of electronic channels and the simplicity of the needed electronics. On the other side, SiPMs present higher quantum efficiency for the scintillation wavelength (≈ 430 nm). In order to discard false-events due to the PMTs photocathode self-emission, the prototype uses 2 PMTs placed at each end of the cell in coincidence mode. The PMTs are optically coupled to the PMMA windows through Saint-Gobain Crystals BC630 optical grease.

3. Simulation details

3.1. Physics list and materials properties

For the calculations presented here, the GEANT4 toolkit [11] was used. In order to comply with the low energy calculations requirement the Livermore physics list (*G4EmLivermorePhysics*) was used, which includes electromagnetic processes as Bremsstrahlung, Coulomb scattering, atomic de-excitation (fluorescence) and other related effects. In these calculations, the properties of Saint-Gobain BCF-10 fibers stated by the manufacturer were employed, a scintillation yield of 8000 photons/MeV for Minimum Ionizing Particles (MIPs) was assumed [10]. This value is however one of the main concerns in these calculations as the energy region of interest is orders of magnitude lower than that of MIPs. Without other low energy data, we assumed a proportionality between energy and the number of produced photons. In order to overcome this lack of information we are planning a measurement of the number of produced photons using low energy electrons. The fiber material proper-

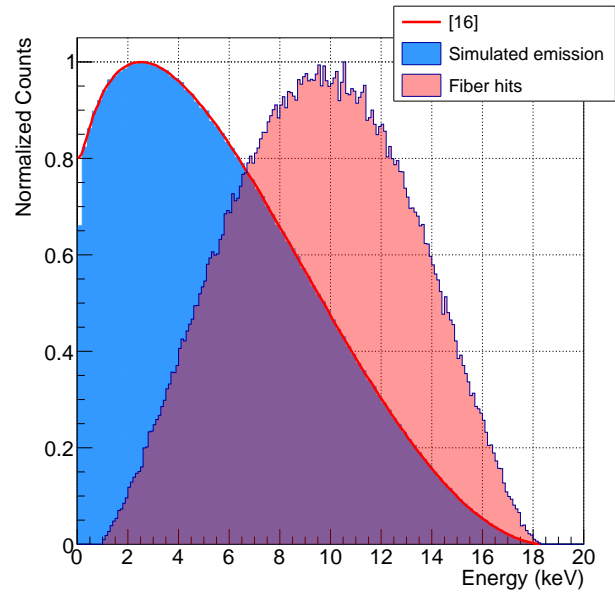


Figure 2: Tritium beta energy distribution (blue) generated with GEANT4 by sampling the distribution obtained from [16] and the corresponding energy distribution (red) of the electrons that deposit energy in the fiber.

ties (polystyrene) was taken from *GEANT4 NIST* database (*G4_POLYSTYRENE*). The fiber emission spectrum was taken from the manufacturer data [10] while the polystyrene light attenuation values were collected from Ref.[12]. The water optical properties were taken from Ref.[13] with exception from the absorption length collected from Ref.[14]. The PMMA (optical windows), teflon and borosilicate glass (PMT windows) optical data were collected from Ref.[12] and a refraction index of 1.46 was employed for the silicon optical grease. The photon detectors (PMTs) selected for their QE and availability in the market were the Hamamatsu R2154-02. The typical quantum efficiency curve was collected from the manufacturer datasheet [15].

3.2. Source simulation

In this section an *ad-hoc* study on the tritium decay and the interaction with a single fiber is carried out. The beta source was considered as a water tube with internal diameter equal to the fiber diameter and a wall thickness of 0.5 mm. The source position was sampled uniformly in the water volume by using the *GeneralParticleSource* (*GPS*) class. The tritium beta emission energy was sampled from Ref. [16]. The results are presented in Figures 2-3. Figure 2 presents the normalized distributions for the sampled tritium beta decay distribution (blue histogram) obtained from the energy distribution given in Ref. [16] (red line). The red histogram represents the initial energy of the electrons released in the water that are able to reach the fiber and deposit energy in it. From the figure it can be observed that there is a shift on the peak position which indicates that the majority of low energy electrons do not reach the fiber, being thermalised in

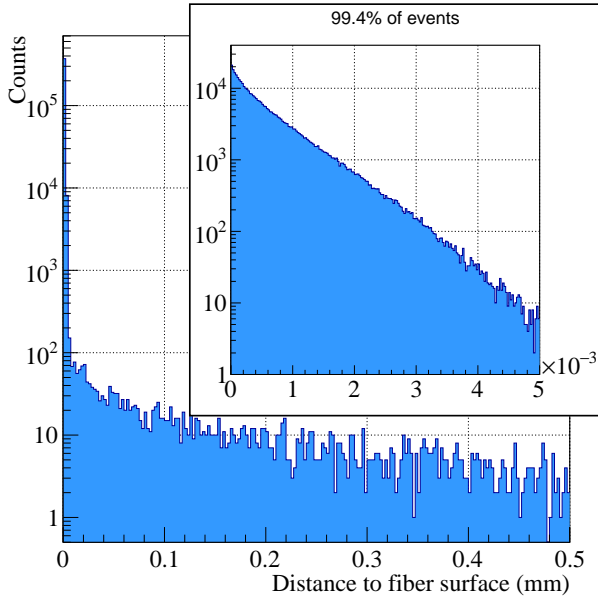


Figure 3: Histogram of the distances between the emission position and fiber surface for detected electrons. The box is a detail (re-binned) of the data below $5 \mu\text{m}$

the water. The peak is now centred at 10 keV with a broad distribution from 1 keV to the maximum energy emission ($Q = 18 \text{ keV}$). It should be noticed that the distributions are normalized to their maximum for better visualization. Figure 3 presents the histogram of the distance between the β emission position and the fiber surface for the events that deposit energy in the fiber. A narrow peak for small distances is observed displayed between 0 and $5 \mu\text{m}$ being in the up-left inset. From the number of entries in the histograms we calculate that the region until $5 \mu\text{m}$ contains 99.4% of the total events, which indicates that the majority of electrons that deposit energy in the fibers are generated at a distance shorter than $5 \mu\text{m}$ from the fiber surface. This result allowed us, in order to reduce computing time, to limit the source thickness (water volume around the fiber) to the $5 \mu\text{m}$ water layer which corresponds to an interaction efficiency (number of events that deposits energy in the fiber normalized to the total number of events generated in the source volume) of 5%. These results are in agreement with the values presented in Refs. [6, 7] showing that the detector efficiency depends on the sensitive surface in contact with water, which in this case corresponds to the number and length of the fibers.

3.3. Optical properties - The quest of Birks' coefficient

Besides the mentioned uncertainty in the scintillation yield in section 3.1, another parameter that determines the light output is the Birks' coefficient for the fibers defined in an empirical formula fitting the expected light yield per unity of path length ($\frac{dL}{dx}$) to the experimental data which are smaller

due to quenching [17]:

$$\frac{dL}{dx} = S \frac{\frac{dE}{dx}}{1 + k_B \frac{dE}{dx}} \quad (1)$$

where, S is the scintillation efficiency, k_B is Birks' coefficient (material dependent) and $\frac{dE}{dx}$ is the energy loss of the particle per unity of path length.

We assume again that the Birks' coefficient for MIPs ($k_B = 0.126 \text{ mm/MeV}$) is valid. This assumption could fail due to a non linear relation between energy deposition and light yield [18] and to the low energy of tritium electrons compared to MIPs. To investigate the importance of Birks' coefficient, the simulated light yield taking for k_B either a null value or the MIPs value was calculated and the results presented in Figure 4. For the case in which Birks' coefficient was considered as zero (red distribution) a peak of 40 photons produced per beta particle interacting in the fiber is found with a wide distribution ranging from 1 to 140 photons. The maximum number of photons value is in agreement with the extrapolated value of the fiber light yield (8000 photons/MeV) for the maximum beta emission energy from tritium (18 keV). When the Birks' coefficient is considered, the expected light reduction is observed: the maximum of the distribution of produced photons peaks at about 10 with a maximum number near 110 photons.

In order to evaluate the effect of the Birks' coefficient in the event detection efficiency (an event is considered as detected when both PMTs produce a signal) we define the *optical detection efficiency* by normalizing the number of detected events to the number of the events which deposit energy in the fiber. When Birks' coefficient was not considered we obtained an *optical detection efficiency* of 87% being reduced to 67% when Birks' coefficient was included.

4. Full detector simulation

After tuning the photon production and beta interaction processes, the full detector was simulated. A 20 cm long detector closed by two PMMA windows (1 cm thick in order to seal the water by radially pressing the teflon tube). The PMTs were optically coupled to the PMMA windows by a 0.5 mm thick layer of optical silicon grease. 341 fibers of 2 mm diameter covered by a $5 \mu\text{m}$ layer of tritiated water were distributed inside a teflon tube of 43 mm of internal diameter of 43 mm fitting the 2" PMTs. All the parameters were considered, e.g., the fiber and water photon absorption, teflon reflectivity and optical surfaces phenomena (reflections and refractions) and PMTs quantum efficiency. An example of an event is show in Figure 5 (obtained from GEANT4). In the figure PMTs are displayed in black at the extremities of the teflon tube (grey). The green lines are the photons paths that, when terminated with a red dot in the PMTs mean a detected photon. The fiber where the beta interaction has occurred is clearly distinguished from the others by the high density of photons paths due to the fiber total internal reflection. The other photon paths are created

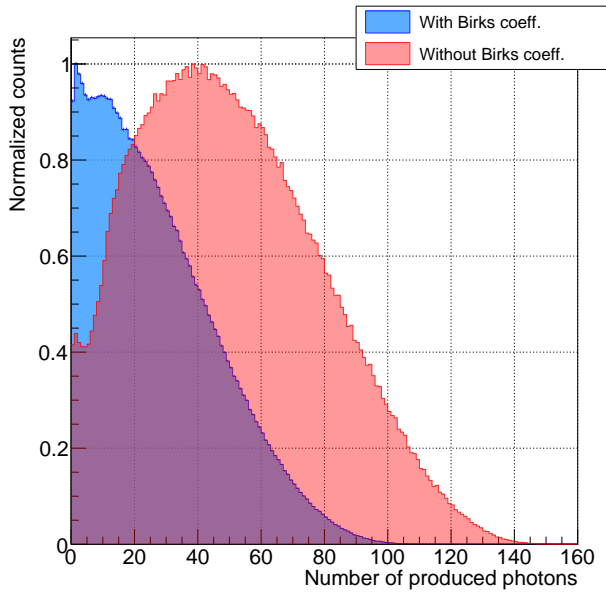


Figure 4: Distribution of scintillation photons produced by the tritium decays in water when interacting with the fiber. Blue: Birks' coefficient considered as $0.126 \cdot \text{mm}/\text{MeV}$. Red: Birks' coefficient considered as $0 \cdot \text{mm}/\text{MeV}$.

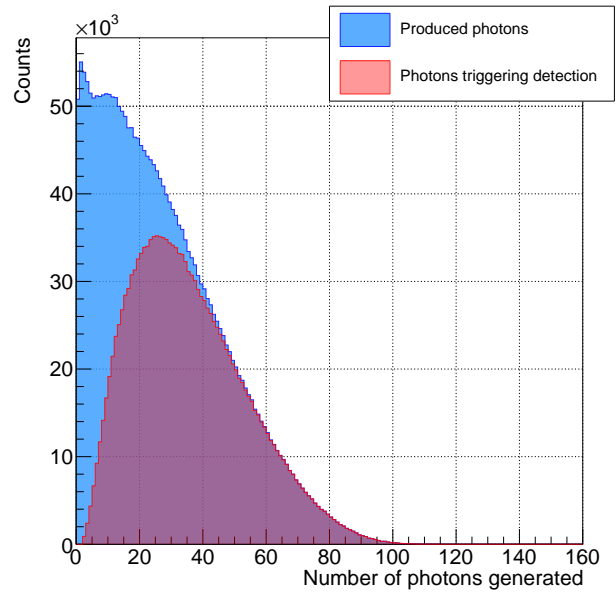


Figure 6: Histograms of the number of produced photons and the number of produced photons when the event is considered as detected

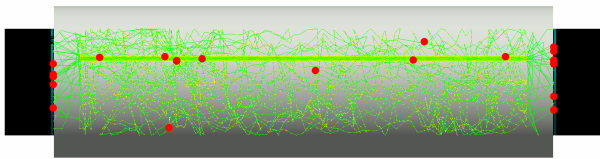


Figure 5: Example of detected events where the red dots are the photons detection positions (in PMTs - black) or optical photon absorption (in the fiber and water regions). Green lines are the optical photons paths

by photons not trapped in the fiber critical angle traveling in water and being reflected in the teflon tube internal wall. Red dots along the fiber and in the water represents the photon absorption position by the materials. By considering the single-photon detection capability of the PMTs, a detection coincidence is counted when both PMTs have at least one single photon detected. The results for 18 cm length fibers are shown in Figure 6 where the distribution of the number of produced photons per event is shown in blue color (as in Figure 4), while in red color are the data for events detected in coincidence. The results reveal that the coincidence detection is peaked for events which produce 25 photons. The fast decreases on the left side of the peak is due to the PMTs quantum efficiency ($\approx 25\%$) and optical losses (absorption). On the right side of the peak the distribution match the blue histogram meaning that in this region, all the produced events are detected.

4.1. The fiber length

From the results presented in Figure Ref.3 and also stated in [7] the detector efficiency depends on the sensitive surface area in contact with the water. Two approaches to increase the surface area are foreseen: Longer fibers (1 m) or a modular system composed by multiple cells. The advantage of the first approach, 1 m long cells is the decrease of the detector price (using just one cell and two PMTs) while the second approach, for the same surface area, the system requires 5 cells and 10 PMTs. On the other side, the advantages of a modular system composed by smaller detectors is the scalability depending on the required sensitivity and a lower photon absorption by the fibers and consequently a higher detection efficiency. In order to study the differences in efficiency between a single cell and a modular system of shorter cells, two sets of data were produced: one for a 1 m long detector and other set for 5 cells of 20 cm length. Two tritium activities were considered: 1 kBq/L and 5 kBq/L for one week of simulated data taking. The results are presented in Figure 7 where blue and red lines correspond to the simulated activities of 1 kBq/L and 5 kBq/L respectively. Solid lines are the data for the 5 cells (20 cm long) while dashed lines are the data for the 1 m long detector. An integration time of 60 min was considered. The results present an increase of the detection efficiency (around 25% relatively) when shorter fibers are used, the difference being due to the fiber self-absorption. It is clear the advantage of a modular system not only due to the increase of the detection efficiency compared to longer fibers but also for the capability of increasing the number of modules in order to fit the required sensitivity.

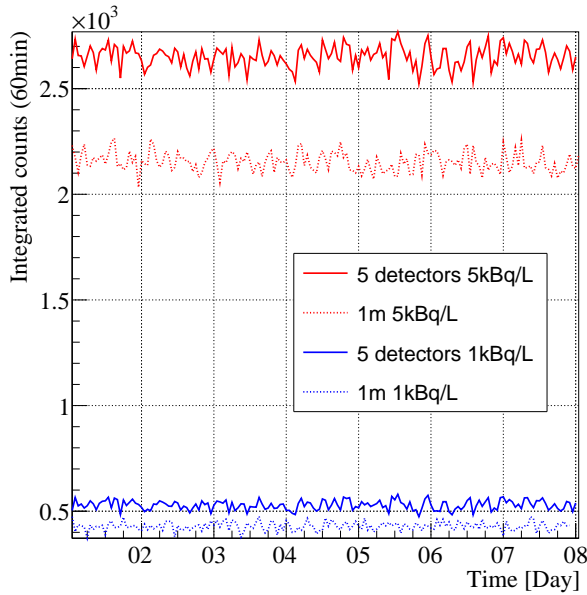


Figure 7: Comparison of the number of coincidences per hour for a 1 m long detector and 5 detectors of 20 cm length.

4.2. Studies on the integration (counting) time

In order to study the effect of the integration time in the system sensitivity two different analysis were carried out. Data obtained for the 5 detectors setup and several source activities ranging from 100 Bq/L to 10 kBq/L corresponding to a week of simulated data taking. In order to get close "real-time" measurement an integration time of 1 min was used. The results are presented in Figure 8 and show the impossibility to distinguish close activity values due to the broad distributions which overlap to activities spaced less than ± 1 kBq/L. The broad distributions are due to the large fluctuations from the combination of the β emission energy spectra (Figure 2), the randomness on decay position relative to the fiber surface (Figure 3) and the system detection efficiency (Figure 6). In order to decrease the statistical fluctuations the data was analysed by using 60 min integration time (what may be denominated as a "quasi-real" time monitoring) and the results are presented in Figure 9. It can be observed that the fluctuations are significantly reduced by increasing the integration time. In this case, for the 5 "cells" setup all simulated activities can be clearly distinguished even for activities as low as 100 and 500 Bq/L. From the data in Figures 8 and 9 it is possible to extract the resolution (eq. 2) of the "measured" activities by fitting a Gaussian function to each data set defined as:

$$Resolution = \frac{FWHM}{centroid} \times 100 (\%) \quad (2)$$

Figure 10 presents the obtained resolution values for 1 and 60 min integration time for the simulated tritium activities (dots) while the lines are fitted functions of the expected sta-

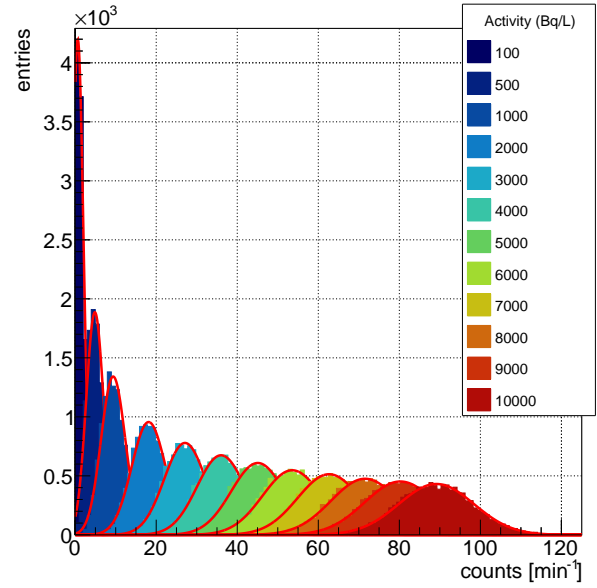


Figure 8: Histograms for the counting rate during a 1 min integration time for several tritium activities in water. Red lines are Gaussian functions fitted to the different activity data set

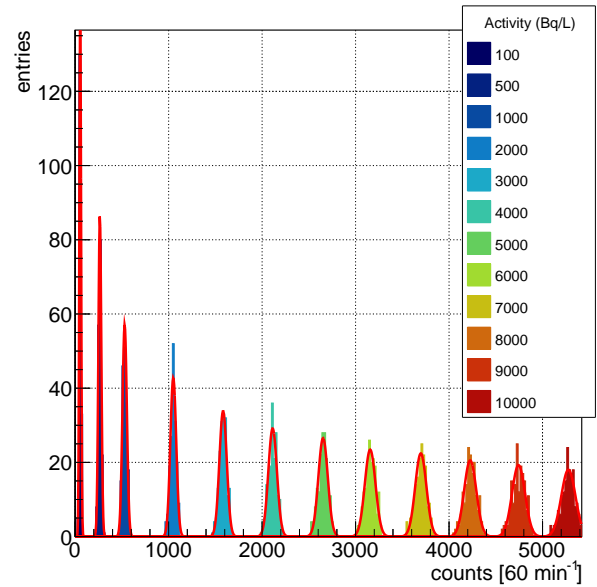


Figure 9: Histograms for the counting rate during a 60 min integration time for several tritium activities in water. Red lines are Gaussian functions fitted to the different activity data set

tistical behaviour as function of the measured quantity:

$$Resolution \propto \frac{1}{\sqrt{X}} \quad (3)$$

As expected from a qualitative analysis of Figures 8-9 and from eq. 3 it can be observed that the resolution for a 60 min

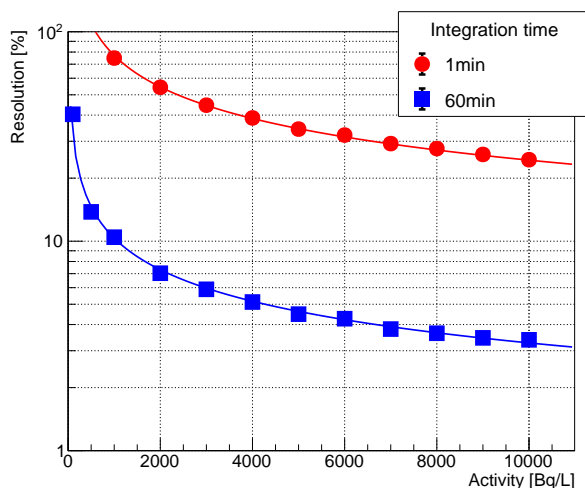


Figure 10: Resolution as a function of the activity for the two considered integration time. The lines correspond to the fitted function $f(x) = C(1/\sqrt{X})$. Error bars are smaller than the marker size

integration is much better when compared to the values obtained for 1 min integration time. For 60 min integration time, resolution values of 40.3% (40 Bq/L) and 3.4% (340 Bq/L) are obtained for activities of 100 Bq/L and 10 kBq/L, respectively.

5. Details on the construction of a prototype

For the construction of the tritium monitor here described two major concerns must be considered: The radiation background (natural and cosmic) and the water contaminants (other radioactive particles than tritium, algae, sediments, etc.). For the natural radioactivity background the use of a lead shield is mandatory (passive shielding) while for the cosmic ray background an anti-coincidence veto based on plastic scintillators (active shielding) must be used. The second concern is the presence of radiative particles, contaminants and algae existing in the water, which may produce fake events while progressively depositing on the fibers surface and disabling the detector sensitivity to low energy beta detection. To avoid these problems the detector must be operated after a water cleaning system which must filter and deionize the water to the required purity levels (conductivity $< 10 \mu\text{S}/\text{cm}$).

In parallel to this work 2 prototypes based on PMTs and SiPMs, including a veto discriminator for cosmic background rejection, have been produced, tested in laboratory and *in situ* (at the discharge channel from Almaraz power plant dam) where a passive shield and a cleaning water system is installed [9]. The prototypes have been constantly monitored being the detection efficiency limited by the cosmic background. A decrease of 400x was observed when introducing the prototypes in the passive shield and tests in the lab have allowed to distinguish tritium activities spaced by 5 kBq/L by just using the passive shield and a single "cell". These re-

sults will be soon published including the electronics design, data acquisition and slow-control of the system.

6. Conclusions

As a main conclusion of this paper, as reported in section 3.2, a single fiber of 2 mm diameter surrounded by a $5 \mu\text{m}$ water layer presents an interaction efficiency of 5%. About a 65% of the events with enough energy in the detector to be recorded, trigger a coincidence in both PMTs (Figure 6) resulting in a system detection efficiency slightly above of 3% for a single fiber. Due to the low interaction efficiency the sensitivity of the detector for low tritium activities must be increased by increasing the detection area, i.e., the number of fibers. The results presented in this work shows the possibility to build an in-water quasi-real-time (60 min time integration) tritium monitor with sensitivity of 100 Bq/L (40 Bq/L resolution) by using 5 cells containing around 350 fibers of 2 mm diameter and 18 cm length. The modular approach of the system allows to increase the sensitivity by including more "cells" in the setup.

7. Acknowledgements

This work was supported by the INTERREG-SUDOE program through the project TRITIUM - SOE1/P4/E0214. C.D.R. Azevedo was supported by Portuguese national funds (OE), through FCT - Fundação para a Ciência e a Tecnologia, I.P., in the scope of the Law 57/2017, of July 19. Part of this work was also developed within the scope of the project i3N, UIDB/50025/2020 & UIDP/50025/2020, financed by national funds through the FCT/MEC.

References

- [1] X. Hou, Tritium and ^{14}C in the environment and nuclear facilities: Sources and analytical methods, *Journal of the Nuclear Fuel Cycle and Waste Technology (JNFCWT)* 16 (2018) 11–39. doi:10.7733/jnfcwt.2018.16.1.11.
- [2] K. J. Hofstetter, H. T. Wilson, Aqueous effluent tritium monitor development, *Fusion Technology* doi:10.13182/fst92-a29786.
- [3] Council directive 2013/51/euratom. URL <https://eur-lex.europa.eu/eli/dir/2013/51/oj>
- [4] K. Hofstetter, Continuous monitoring for tritium in aqueous effluents at srs using solid scintillators, *Transactions of the American Nuclear Society; (United States)* 69.
- [5] K. J. Hofstetter, Continuous aqueous tritium monitoring, *Fusion Technology* doi:10.13182/fst95-a30629.
- [6] M. Rathnakaran, R. Ravetkar, R. Samant, et al., A real-time tritium-in-water monitor for measurement of heavy water leak to the secondary coolant, in: *IRPA-10 Conf. Rec., Japan Health Physics Society, 2000*, p. 1. URL https://inis.iaea.org/search/search.aspx?orig_q=RN:32015986
- [7] J. W. Berthold III, L. A. Jeffers, Method for in-situ detection of tritium in water, 1999, pp. 434–442. doi:10.1117/12.372989. URL <http://proceedings.spiedigitallibrary.org/proceeding.aspx?articleid=909924>
- [8] V sudoe interreg program. URL <https://www.interreg-sudoe.eu/gbr/projects/the-approved-projects/158-design-construction-and-commissioning-of-a-low-level-tritium-monitor-for-w>

- [9] C. D. Azevedo, A. Baeza, M. Bras, et al., TRITIUM - A Real-Time Tritium Monitor System for Water Quality Surveillance, in: 2018 IEEE Nuclear Science Symposium and Medical Imaging Conference, NSS/MIC 2018 - Proceedings, 2018. arXiv:1902.05456, doi: 10.1109/NSSMIC.2018.8824700.
- [10] Saint-Gobain Crystals, Scintillating Optical Fibers.
URL <https://www.crystals.saint-gobain.com/sites/imdf.crystals.com/files/documents/fiber-brochure.pdf>
- [11] GEANT4.
URL <http://geant4.cern.ch/>
- [12] J. Argyriades, R. Arnold, C. Augier, et al., Spectral modeling of scintillator for the NEMO-3 and SuperNEMO detectors, Nuclear Instruments and Methods in Physics Research Section A: Accelerators, Spectrometers, Detectors and Associated Equipment 625 (1) (2011) 20–28. doi:10.1016/j.nima.2010.09.027.
URL <https://linkinghub.elsevier.com/retrieve/pii/S0168900210020206>
- [13] J. Armstrong, Geant4 OpNovice example .
URL http://www.apc.univ-paris7.fr/~franco/g4doxy4.10/html/_op_novice_detector_construction_8cc_source.html
- [14] H. Buiteveld, J. H. M. Hakvoort, M. Donze, Optical properties of pure water, in: J. S. Jaffe (Ed.), Ocean Optics XII, Vol. 2258, International Society for Optics and Photonics, SPIE, 1994, pp. 174 – 183. doi: 10.1117/12.190060.
URL <https://doi.org/10.1117/12.190060>
- [15] H. P. K.K, R2154-02 PMT.
URL https://www.hamamatsu.com/resources/pdf/etd/R2154-02_TPMH1089E.pdf
- [16] S. Mertens, T. Lasserre, S. Groh, et al., Sensitivity of next-generation tritium beta-decay experiments for keV-scale sterile neutrinos, Journal of Cosmology and Astroparticle Physics 2015 (02) (2015) 020–020. doi:10.1088/1475-7516/2015/02/020.
URL <http://stacks.iop.org/1475-7516/2015/i=02/a=020?key=crossref.95e02cc952a84301b2bec83e25d43926>
- [17] G. F. Knoll, Radiation detection and measurement, 3rd Edition, John Wiley & Sons, New York, 2000.
- [18] E. Dietz-Laursonn, Peculiarities in the Simulation of Optical Physics with Geant4 arXiv:1612.05162.
URL <http://arxiv.org/abs/1612.05162>